

## EM TRANSMISSION RESPONSE OF MICROSTRIP NOTCH FILTER ON OBLIQUELY MAGNETIZED MAGNETODIELECTRIC SUBSTRATE IN X-BAND UNDER INFLUENCE OF LOW MAGNITUDE OF EXTERNAL DC MAGNETIC FIELD

S. Borah and N. S. Bhattacharyya\*

Microwave Engineering Laboratory, Department of Physics, School of Science and Technology, Tezpur University, Tezpur 784 028, Assam, India

**Abstract**—A tunable microwave notch filter is developed on magneto-dielectric material having low saturation magnetization to attain low external dc magnetic field for biasing. A simple microstrip line at 10 GHz is developed on nickel ferrite/low density polyethylene nanocomposite system as substrates and its microwave transmission response is studied in X-band. Composite system is developed by dispersing nano sized nickel ferrite ( $\sim 6.63$  nm) in low density polyethylene to obtain a homogeneous flexible substrate. Saturation magnetization of 4% volume fraction of the composite is found to be 1.8745 emu/g. Tunability of Q value and insertion loss is studied with magnitude of external dc magnetic field and at different angles of its orientation with the axial plane. A very low field up to 250 G is sufficient to tune the selectivity. An insertion loss of  $\sim -30$  dB and  $Q \sim 375$  at 10.2 GHz is observed. The interaction of magneto static modes with orientation of the applied dc magnetic bias with respect to *rf* magnetic field is discussed with couple mode theory. Good cut-off behaviour of more than 28 dB is observed at magnetic field angles from  $23.52^\circ$  to  $34.21^\circ$ . The experimental and theoretical couplings show close proximity.

### 1. INTRODUCTION

Gyrotropic properties of ferrites have been long exploited to develop microwave devices which are non-reciprocal. External magnetic tuning

---

*Received 1 August 2011, Accepted 21 September 2011, Scheduled 22 September 2011*

\* Corresponding author: Nidhi Saxena Bhattacharyya (nidhisbhatta@gmail.com).

of MIC devices fabricated on the ferrite substrate finds applications for removal of spurious frequencies and is the need of present day mobile and satellite communication systems [1–5]. Most of the magnetically tuned microwave devices reported have been realized on bulk ferrites and require sufficiently large external dc magnetic field to alter the device  $S$ -parameters. Nano sized ferrites are reported to have low saturation magnetization, and hence a small external dc magnetic field should be sufficient to select/deselect the transmission band of passive  $rf$  components fabricated on them [6–8].

In this investigation, band selectivity of the microstrip line is studied with magnitude of external dc magnetic field bias and its orientation w.r.t. pumped  $rf$  magnetic field on a new class of low loss magnetodielectric nanocomposite substrate. For fast transition in band selection, the planar device has to show a quick on/off response with variation of external dc magnetic field. For this purpose,  $Ni^{2+}$  ferrite is selected because of its soft magnetic properties. The substrate is synthesized by reinforcing nano sized  $NiFe_2O_4$  particles in low density polyethylene matrix. The  $NiFe_2O_4$ -LDPE composite offers low hysteresis losses and low domain-wall displacement, as the ferrite nanoparticles approach single crystal domains and also the skin effect is suppressed in the composite sample as the average size of the  $NiFe_2O_4$  nanoparticles is much smaller than the skin depth in 3d ferromagnetic metals, at microwave frequencies [9]. The polymer matrix, in the composite, provides additional dimensional flexibility. The magneto-dielectric material is engineered to develop the geometry. The magnetostatic modes generated in the planar transmission line system are analyzed using coupled mode theory [10].

## 2. EXPERIMENT

### 2.1. Material Synthesis

The substrate is fabricated by reinforcing 2% and 4% volume fraction of ( $NiFe_2O_4$ ) nano particles into LDPE matrix. Nickel ferrite nanoparticles are prepared by wet synthesis method by annealing the precipitate precursor powders at 400°C temperatures [11].

An improved thermal conductivity, of value 0.0156 W/cmK, is observed for 4% v.f. of the magnetodielectric composite as compared to 0.0108 W/cmK for 2% VF. The 4% volume fraction of the magnetodielectric composite is chosen as the substrate for microstrip line for further study because of its better heat dissipation capability. Thermal conductivity of the magnetodielectric composite is measured by Lee's method. The water absorbance study, carried out for 48 hrs, shows the composite to be hydrophobic with 0% water absorbance.

### 2.2. Microstructural Study of the Magnetic Nanoparticles

The average crystallite size of the  $\text{NiFe}_2\text{O}_4$  nanoparticles, annealed at  $400^\circ\text{C}$ , is determined from X-ray diffraction (XRD) study and is found to be about 6.63 nm [11]. Transmission electron micrographs (TEM) of the ferrite particles are taken to see the microstructural properties like shape and size using JEOL-TEM-100 CXII (Collision Coated Copper Grids) as shown in Fig. 1(a). Most of the particles appear almost spherical in shape as seen in the TEM images. Some moderate agglomerations of particles are present in the images, at higher resolution. This is possibly due to interaction of the dispersed particles with the intense electron beam, as resolution increases.

### 2.3. Magnetic Measurement of the Magnetodielectric Composite material

Magnetization properties are studied using Vibrating Sample Magnetometer (VSM), Make: Lake Shore Cryotronics Inc., USA, Model: 7410. Fig. 1(b) shows the plot of magnetization versus magnetic field ( $M$ - $H$  loop) at room temperature for 4% volume fraction of  $\text{NiFe}_2\text{O}_4$  nanoparticles, reinforced in LDPE matrix. The plot of  $M$  vs.  $H$  with magnification close to the origin and saturation is shown in Fig. 1(b) as inset (a) and (b) respectively. The numerical values estimated are shown in Table 1.

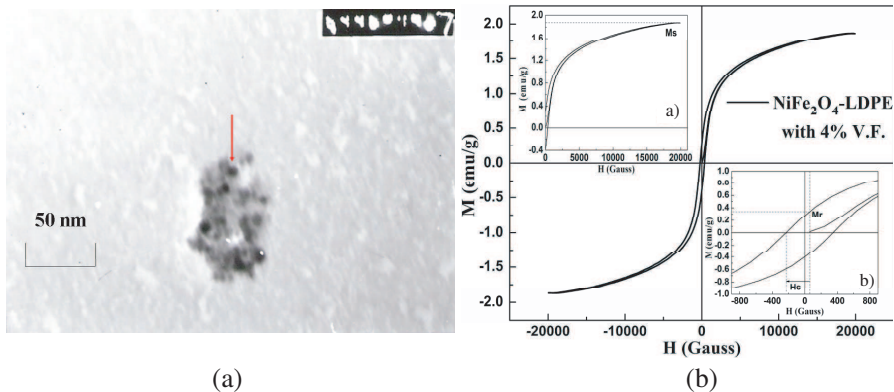


**Figure 1.** (a) Transmission electron micrograph of  $\text{NiFe}_2\text{O}_4$  nanoparticles annealed at  $400^\circ\text{C}$  temperature. (b) Magnetization versus magnetic field ( $M$ - $H$  loop) at room temperature for the 4% volume fraction of  $\text{NiFe}_2\text{O}_4$ -LDPE composite (nanoparticles annealed at  $400^\circ\text{C}$ ) with enlargement near a) origin and b) saturation.

**Table 1.** Various parameters estimated from the magnetization curve of the nickel ferrite-LDPE composite.

Saturation magnetization ( $M_s$ )	Remanent magnetization ( $M_r$ )	Coercivity ( $H_c$ )	Squareness ( $S_r = M_r/M_s$ )
1.8745 emu/g	0.337 emu/g	273.344 G	0.180

Density of the composite is evaluated by Archimedes' principle and is found to be 0.8 g/cc. In CGS unit, the  $4\pi M_s$  value is found to be 18.835 G for the 4% volume fraction of the composite.

## 2.4. Microstrip Line

The design parameters for the microstrip line at 10 GHz, are determined from the design described in literature [12–20]. The dispersive effective permittivity,  $\varepsilon_{eff}(f)$ , and permeability  $\mu_{eff}(f)$ , of the microstrip line geometry for demagnetized state, are computed from the following equations as [15, 18]

$$\varepsilon_{eff}(f) = \varepsilon_r - \frac{\varepsilon_r - \varepsilon_{eff}}{1 + \left(\frac{h}{Z_0}\right)^{1.33} (0.43f^2 - 0.009f^3)} \quad (1)$$

$$\mu_{eff}(f) = \frac{1}{3} + \frac{2}{3} \left[ (1 - p^2)^{1/2} \right] \text{ where } p = \frac{\gamma 4\pi M_s}{\omega} \quad (2)$$

where  $\omega$  is the operating frequency in rad/sec and  $\gamma$  is the gyromagnetic ratio. The symbols, in (1), have same meaning as mentioned in [18]. The complex permittivity,  $\varepsilon_r$ , and permeability,  $\mu_r$ , of the magnetodielectric substrate material (at the design frequency) are evaluated using shielded conductor backed coplanar waveguide technique [21].

The guided wavelength of the magnetodielectric substrate is determined by substituting the values of (1) and (2) in the equation given below

$$\lambda_g = \frac{\lambda_0}{\sqrt{\mu_{eff}(f) \varepsilon_{eff}(f)}} \quad (3)$$

where  $\lambda_0$  is the wavelength of the designed frequency.

The microstrip line is designed at 10 GHz frequency, using the parameters tabulated in Table 2. Fabrication of copper line on the NiFe<sub>2</sub>O<sub>4</sub>-LDPE substrate is performed in two steps by rolling technique [22]. A thin layer of cyanoacrylate epoxy resin (CER), of thickness less than 20 micron (99.95% less than the probing

wavelength), is used on both sides of the substrate as an adhesive. It is observed with the cavity resonator method that the loaded frequency of the substrate does not shift its position on brushing the CER adhesive on both sides of the substrate. Copper sheet of thickness 0.15 mm is placed on both sides of the substrate, and rolled at pressure 6 torr for one hour, to obtain the metallized substrate. Fig. 2 shows the schematic of the microstrip line. An external dc magnetic field ( $\mu_0 H_0$ ) is applied at different  $\theta$  w.r.t. axial plane ( $X$ - $Y$  plane), whereas the electromagnetic wave is propagated along the  $Z$ -axis.

### 3. RESULTS

#### 3.1. Microstrip Line Transmission Response

Microstrip line drawn on  $\text{NiFe}_2\text{O}_4$ -LDPE composite substrate shows high insertion loss for low external dc magnetic field strength unlike, YIG and other bulk ferrites where the magnetic strength of the order of few kilo gauss is required for tunability [23].

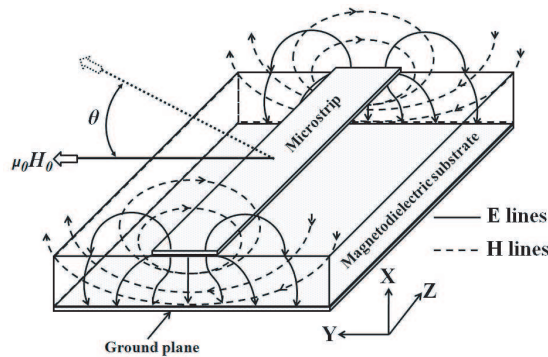


**Figure 2.** Schematic of microstrip line geometry arbitrarily magnetized in the  $XZ$  plane.

**Table 2.** Design parameters of the microstrip line, fabricated on the magnetodielectric substrate at 10 GHz frequency.

Design frequency (GHz)	Height of the substrate (mm)	W/h	$4\pi M_s$ (G)	$\mu_{eff}$ (f)	$\epsilon_{eff}$ (f)	$\lambda_g$ (mm)	Length of the microstrip line (mm)
10	1.1	3.32	18.835	1.0	2.074	0.208	16

$S_{21}$ -parameter is measured using an automated PC-based system developed in the laboratory [24]. The measurement system has frequency least-count of 0.001 GHz. Measurements are carried out over a range from 9.500 to 12.045 GHz at room temperature.

Figure 3(a) shows the transmission characteristics of the microstrip line under the influence of external magnetic field ( $\mu_0 H_0$ ). The insertion values (Figs. 3(a) and 3(b)) for 800 G and 1 kG external dc magnetic merges for both angles (a)  $\theta = 0^\circ$  and (b)  $\theta = 90^\circ$  orientation and cannot be resolved even after magnifying the graph. This is because, low saturation magnetization of the substrate makes the insertion loss unaffected for values of  $\mu_0 H_0 > 800$  G. In absence of external bias, two notches at 9.91 GHz and 10.05 GHz having insertion

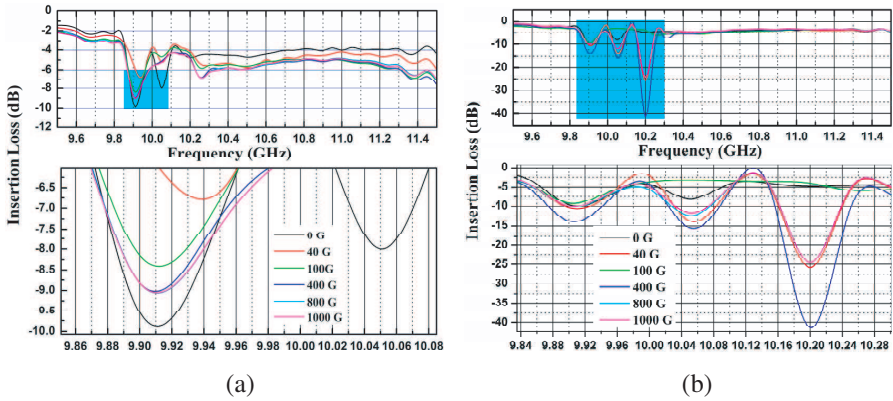


**Figure 3.** Insertion loss of the microstrip line geometry under external dc magnetic field applied along  $XY$  plane at an angle (a)  $\theta = 0^\circ$  and (b)  $\theta = 90^\circ$ .

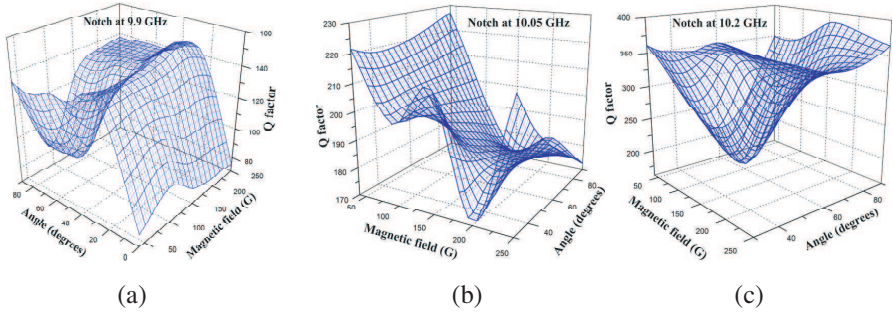


**Figure 4.** Tunability of  $Q$ -factor of the microstrip line as a function of applied  $\mu_0 H_0$  and  $\theta$  measured from the notch at (a) 9.9 GHz, (b) 10.05 GHz and (c) 10.2 GHz.

loss values  $-9.871$  dB and  $-7.987$  dB, respectively, are observed. The shift in the design frequency from 10 GHz to 9.91 GHz is observed due to uncertainty of 0.5% in the measured complex permittivity values at the design frequency [21].

On increasing the strength of  $\mu_0 H_0$  to 400 G along  $Y$ -axis of the microstrip line geometry  $\theta = 0^\circ$ , it is observed that 9.91 GHz notch does not show much variation in the insertion loss. Orienting the 400 G magnitude external magnetic field along  $X$ -axis ( $\theta = 90^\circ$ ), a notch of  $-41.33$  dB at 10.2 GHz is observed (Fig. 3(b)).

To observe how precise variation of magnetic field changes the insertion loss, the  $Q$ -factor of the microstrip line as a function of magnitude of applied  $\mu_0 H_0$ , over the range of 30 G to 250 G in steps of 10 G at orientation of  $0^\circ$ ,  $30^\circ$ ,  $45^\circ$ ,  $60^\circ$  and  $90^\circ$  are plotted in Figs. 4(a), 4(b) and 4(c).

The notch generated at 10.2 GHz frequency at  $90^\circ$  orientation shows highest value of  $Q = 375$ , having 3 dB bandwidth of 26 MHz and is studied for transmission response in two ways

- (a) Fixing the inclination and changing the magnitude of external  $\mu_0 H_0$ . Fig. 5(a) shows insertion loss plots with small variation of  $\mu_0 H_0$  within 30 G to 250 G, applied at fixed angles to the axial plane.
- (b) Keeping the magnitude of  $\mu_0 H_0$  fixed and altering the angle of inclination,  $\theta$ . Fig. 5(b) shows the insertion loss notch of the line with changing  $\theta$  values for fixed  $\mu_0 H_0$ .

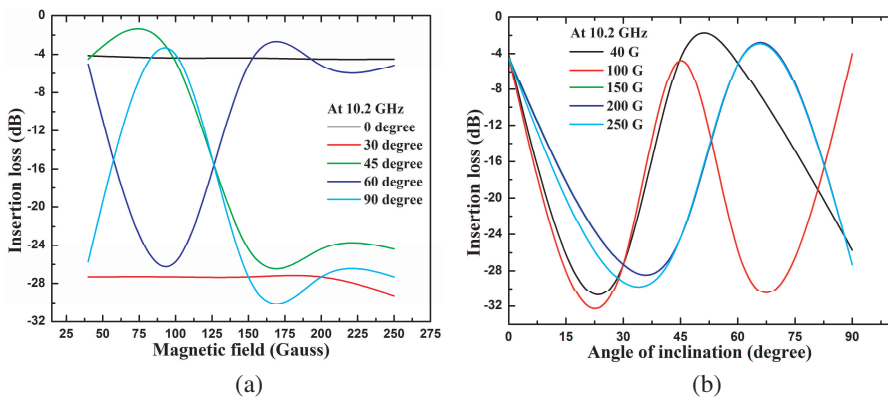


**Figure 5.** Variation of insertion loss of the microstrip line at 10.2 GHz notch with change in (a)  $\mu_0 H_0$  and (b)  $\theta$ .

## 4. DISCUSSION

### 4.1. Transmission Response with Varying Magnitude of dc Magnetic Field

NiFe<sub>2</sub>O<sub>4</sub>-LDPE composite system shows small saturation magnetization,  $M_s = 1.8745$  emu/g (Section 2.3). The magnetic inclusions approaches single domain as the size of the particles approaches nano scale [25, 26]. The NiFe<sub>2</sub>O<sub>4</sub> nanoparticles are immobilized in the LDPE matrix throughout the volume of the substrate which disallows agglomeration of the filler particles. The diamagnetic phase of the polymer between the two magnetic particles lowers the exchange interaction phenomenon among the ferrite nanoparticles [27]. The low interparticle exchange interactions results in reduction of saturation magnetization value of the magneto-dielectric composite material and the magnitude of external dc magnetic field required for magnetizing the substrate is also low. In the present investigation, it is observed that (Section 3.1) small magnitude of external  $\mu_0 H_0$  is sufficient for changing the transmission line response of microstrip line on NiFe<sub>2</sub>O<sub>4</sub>-LDPE substrate.

With application of external magnetic bias, at some value of  $\mu_0 H_0$ , the magnetization of the magneto-dielectric composite system reaches the saturation level. Beyond this value, any further increase in the magnetic field has little or no effect on the alignment of magnetic moments of NiFe<sub>2</sub>O<sub>4</sub> nanoparticles and the magnetization reaches a steady value, and the insertion loss value does not reduce further. However, with the increase in external magnetic field beyond 400 G, notch characteristic reduces from  $-41.33$  dB to  $-24.38$  dB (Fig. 3(b)). With increase in external dc magnetic field beyond the saturation level, the permeability for the substrate becomes more negative and the penetration of the magnetic field component into the ferrite decreases [28]. This results in less concentration of electromagnetic energy in the ferrite and subsequent decrease in the magnetic loss. Differential coupling of the longitudinal  $rf$  magnetic field decreases due to low magnetic loss and hence the insertion loss increases allowing the transmission of the  $rf$  power through the microstrip line.

### 4.2. Transmission Response by Altering Angle of Inclination

The variation of insertion loss with changing  $\theta$  can be explained by coupled mode theory and is based on parallel plate transmission mode [10]. The dominant mode of electromagnetic wave propagation in a microstrip transmission line, under unperturbed condition, is quasi TEM. At higher frequencies, TE and TM modes exist separately in

the microstrip line geometry under study. In the presence of external dc magnetic field two magnetostatic modes are produced one at the ferrite-air interface and the second mode is concentrated near the ferrite-metal interface [29]. As the angle of inclination of external  $\mu_0 H_0$  changes from  $0^\circ$  to  $90^\circ$  in the  $X$ - $Y$  plane (Fig. 2), the non diagonal components of the permeability tensor, given by (4), contributes in the coupling between the TE and TM mode.

$$\hat{\mu} = \begin{bmatrix} \mu_{11} & j\mu_{12} & \delta\mu_{13} \\ -j\mu_{21} & \mu_{22} & j\gamma\mu_{23} \\ \delta\mu_{31} & -j\delta\mu_{32} & \mu_{33} \end{bmatrix} \quad (4)$$

The angles where the phase matching between the magnetostatic modes and TEM mode occurs, gives the maximum coupling [10, 30]. The coupling of TM to magnetostatic modes and TE to TEM modes are determined in terms of the coupling coefficients  $C_{ab}$  and  $C_{ba}$ , derived from couple mode equation as [30, 31]

$$C_{ab} = \frac{\delta AB}{4(\mu_{11}\mu_{12} - \mu_{12}^2)} \left[ C_0 \pm (\mu_{13}\mu_{12} + \mu_{23}\mu_{11}) \sinh k'_x s \right] \quad (5)$$

$$C_{ba} = \frac{\delta AB}{4(\mu_{11}\mu_{12} - \mu_{12}^2)} \left[ C_0 \pm \frac{\mu_{12}}{\mu_{22}} (\mu_{13}\mu_{22} + \mu_{12}\mu_{23}) \sinh k'_x s \right] \quad (6)$$

where

$$C_0 = \frac{\beta}{k'_x} (\mu_{22}\mu_{13} + \mu_{12}\mu_{23}) (\cosh k'_x s - 1) \quad (7)$$

$$k'_x = \sqrt{\frac{1}{\mu_{11}} [\beta^2 \mu_{22} - \omega^2 \varepsilon_0 \varepsilon_r \mu_0 (\mu_{11}\mu_{22} - \mu_{12}^2)]} \quad (8)$$

$$\mu = \frac{\omega_0^2 - \omega^2}{\omega_h^2 - \omega^2}, \quad k = \frac{\omega \gamma \mu_0 M_0}{\omega_h^2 - \omega^2}, \quad (9)$$

$$\omega_h = \gamma \mu_0 H_0 \quad \text{and} \quad \omega_0 = \gamma \mu_0 \sqrt{H_0 (H_0 + M_0)}$$

Figure 6 shows plot of  $C_{ab}$  and  $C_{ba}$  computed for the microstrip line on NiFe<sub>2</sub>O<sub>4</sub>-LDPE composite. At  $\theta = 0^\circ$ , the coupling coefficients are zero showing weak interaction between TE and TM modes which propagates separately. These two modes with nonzero cut off frequencies may generate two separate notches, as observed in Fig. 3(a), in absence of external bias field.

Theoretical and experimental angles of inclination for different magnitude of external magnetic field, shown in Table 2, shows close proximity. Experimentally minimum insertion losses are observed at the angles where maximum coupling is occurring (Table 3). Good cut-off behaviour of more than 28 dB is observed over the external magnetic field range from 40 G to 250 G and is caused by coupling between TEM and magnetostatic modes.

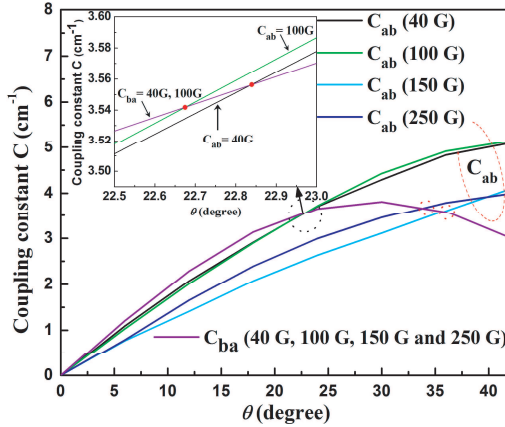


**Figure 6.** Coupling coefficients as a function of angle of inclination of fixed magnitude of applied dc magnetic field w.r.t.  $rf$  magnetic field direction.

**Table 3.** Coupling constants determined from couple mode theory to validate the experimental results.

External magnetic field (G)	From couple mode theory		From experimental results	
	Angle of inclination ( $\theta^0$ )	Coupling constant ( $C \text{ cm}^{-1}$ )	Insertion loss (dB)	Angle of inclination ( $\theta^0$ )
40	22.84	3.56	-30.74	23.52
100	22.67	3.54	-32.25	22.54
150	35.96	3.57	-28.46	35.90
250	34.03	3.64	-29.80	34.21

## 5. CONCLUSION

In this work, microstrip line transmission response on partially magnetized  $\text{NiFe}_2\text{O}_4$ -LDPE nano composite material is studied over X-band. Low saturation magnetization of the composite ( $M_s = 1.8745 \text{ emu/g}$ ) allows us to tune the device at low external magnetic field unlike bulk ferrites. The microstrip line drawn on the magneto dielectric substrate shows a good notch filter characteristic of 30 dB and good band selectivity ( $Q = 375$ ) having 3 dB bandwidth of 26 MHz at 10.2 GHz. The designed transmission line shows tunability with magnitude and changing angle of interaction between dc magnetic applied field and  $rf$  field. Couple mode theory explains

the interaction between TEM and magnetostatic modes, showing the maximum coupling takes between  $22.84^\circ$  and  $34.03^\circ$ , and shows good experimental matching. The results show promising applications of  $\text{NiFe}_2\text{O}_4$ -LDPE composite substrate, as replacement of bulk ferrites, in tunable microstrip band selective filters under influence of low external dc magnetic field.

## REFERENCES

1. Miranda, F. A., G. Subramanyam, F. W. Van Keuls, R. R. Romanofsky, J. D. Warner, and C. H. Muller, "Design and development of ferroelectric tunable microwave components for Ku- and K-band satellite communication systems," *IEEE Trans. on Microwave Theory and Tech.*, Vol. 48, No. 7, 1181–1189, Jul. 2000.
2. Dionne, G. F. and D. E. Oates, "Tunability of microstrip finite resonator in the partially magnetized state," *IEEE Trans. on Magn.*, Vol. 33, 3421–3423, Sept. 1997.
3. Barbarino, S. and F. Consoli, "UWB circular slot antenna provided with an inverted-l notch filter for the 5 GHz WLAN band," *Progress In Electromagnetics Research*, Vol. 104, 1–13, 2010.
4. Hsiao, P. Y. and R. M. Weng, "Compact open-loop UWB filter with notched band," *Progress In Electromagnetics Research Letters*, Vol. 7, 149–159, 2009.
5. Huang, J. Q., Q. X. Chu, and C. Y. Liu, "Compact UWB filter based on surface-coupled structure with dual notched bands," *Progress In Electromagnetics Research*, Vol. 106, 311–319, 2010.
6. Huynen, I., B. Stockbroeckx, and G. Verstraeten, "An efficient energetic variational principle for modeling one-port lossy gyrotropic YIG Straight Edge Resonators," *IEEE Trans. on Microwave Theory and Tech.*, Vol. 46, No. 7, 932–939, Jul. 1998.
7. León, G., R. R. Boix, and F. Medina, "Efficient full-wave characterization of microstrip lines fabricated on magnetized ferrites with arbitrarily oriented bias field," *Journal Electromagnetic Waves and Applications*, Vol. 15, No. 2, 223–251, 2001.
8. Morales, C., J. Dewdney, S. Pal, S. Skidmore, K. Stojak, H. Srikanth, T. Weller, and J. Wang, "Tunable magneto-dielectric polymer nanocomposites for microwave applications," *IEEE Trans. on Microwave Theory and Tech.*, Vol. 59, No. 2, 302–310, Feb. 2011.

9. Gao, B., L. Qiao, J. Wang, Q. Liu, F. Li, J. Feng, and D. Xue, "Microwave absorption properties of the Ni nanowires composite," *J. Phys. D: Appl. Phys.*, Vol. 41, No. 235005, 1–5, Nov. 2008.
10. Yariv, A., "Coupled-mode theory for guided-wave optics," *IEEE J. of Quantum Electronics*, Vol. 9, No. 9, 919–933, Sept. 1973.
11. Borah, S. and N. S. Bhattacharyya, "GCPWG technique for measurement of dielectric properties of magneto-polymer composite at microwave frequencies," *Proc. IEEE*, D.O.I. 10.1109/AEMC.2009.5430594, 2010.
12. Pucel, R. A. and D. J. Masse, "Microstrip propagation on magnetic substrates — Part I: Design theory," *IEEE Trans. on Microwave Theory and Tech.*, Vol. 20, No. 5, 304–308, May 1972.
13. Kaneki, T., "Analysis of linear microstrip using an arbitrary ferromagnetic substance as the substrate," *Electronics Lett.*, Vol. 5, No. 19, 463, Sept. 1969.
14. Collins, R. E., *Field Theory of Guided Waves*, McGraw Hill, 152, 1960.
15. Pucel, R. A. and D. J. Masse, "Microstrip propagation on magnetic substrates — Part II: Experiment," *IEEE Trans. on Microwave Theory and Tech.*, Vol. 20, 309–313, May 1972.
16. Wheeler, H. A., "Transmission-line properties of parallel strips separated by a dielectric sheet," *IEEE Trans. on Microwave Theory and Tech.*, Vol. 13, 172–185, 1965.
17. Hammerstad, E. and Ø. Jensen, "Accurate models for microstrip computer-aided design," *Symposium on Microwave Theory and Tech.*, 407–409, Jun. 1980.
18. Edwards, T. C. and R. P. Owens, "2–18-GHz dispersion measurements on 10–100  $\Omega$  microstrip lines on sapphire," *IEEE Trans. on Microwave Theory and Tech.*, Vol. 24, No. 8, 506–513, Aug. 1976.
19. Schneider, M. V., "Microstrip lines for microwave integrated circuits," *The Bell System Technical Journal*, Vol. 48, 1421–1444, May. 1969.
20. Pramanick, P. and P. Bhartia, "An accurate description of dispersion in microstrip," *Microwave Journal*, 89–96, Dec. 1983.
21. Borah, S. and N. S. Bhattacharyya, "Broadband measurement of complex permittivity of composite at microwave frequencies using scalar scattering parameters," *Progress In Electromagnetics Research M*, Vol. 13, 53–68, 2010.
22. Laverghetta, T. S., *Microwave Materials and Fabrication Techniques*, 3rd edition, Artech House, 2002.

23. Salahun, E., G. Tanne, and P. Queffelec, "Enhancement of design parameters for tunable ferromagnetic composite-based microwave devices: application to filtering devices," *IEEE Trans. Microw. Theory Tech.: Microwave Symposium Digest*, Vol. 3, Nos. 6–11, 1911–1914, Jun. 2004.
24. Deka, J. R., N. S. Bhattacharyya, and S. Bhattacharyya, "Development of low cost automated PC-based insertion loss measurement setup using a simple source and detector in X-band," *IETE Tech. Rev.*, Vol 22, 425, 2005.
25. Jacobs, I. S. and C. P. Bean, "An approach to elongated fine-particle magnets," *Phys. Rev.*, Vol. 100, No. 4, 1060–1067, 1955.
26. Morrish, A. H. and K. Haneda, "Magnetic structure of small  $\text{NiFe}_2\text{O}_4$  particles," *J. Appl. Phys.*, Vol. 52, No. 3, 2496–2498, 1981.
27. Nathani, H., S. Gubbala, and R. D. K. Misra, "Magnetic behavior of nickel ferrite–polyethylene nanocomposites synthesized by mechanical milling process," *Materials Science and Engineering B*, Vol. 111, 95–100, 2004.
28. Lax, B., "Frequency and loss characteristics of microwave ferrite devices," *Proc. IRE*, Vol. 44, 1368–1386, Oct. 1956.
29. Gerson, I. J. and J. S. Nandan, "Surface electromagnetic modes of a ferrite slab," *IEEE Trans. on Microwave Theory and Tech.*, Vol. 22, No. 8, 757–763, Aug. 1974.
30. Tsutsumi, M. and S. Tamura, "Microstrip line filters using yttrium iron garnet film," *IEEE Trans. on Microwave Theory and Tech.*, Vol. 40, No. 2, 400–402, Feb. 1992.
31. Ishak, W. and K. W. Chang, "Tunable microwave resonators using magnetostatic wave in YIG films," *IEEE Trans. on Microwave Theory and Tech.*, Vol. 34, No. 12, 1383–1393, Dec. 1986.